

## Simulation of magnetic field effect on a seed embryo cell

A. Socorro<sup>1</sup> and F. García<sup>2</sup>

<sup>1</sup>Department of Plant Physiology and Postharvest, Institute of Fundamental Researches on Tropical Agriculture A. Von Humboldt, INIFAT Calle 2 esq. 1 Santiago de Las Vegas, CP 17200, Ciudad de La Habana, Cuba

<sup>2</sup>Department of Physics, Ciego de Ávila University, Carretera de Moron, Km. 9 Ciego de Avila, Cuba

Received March 28, 2011; accepted April 13, 2011

**A b s t r a c t.** The plant seed embryo tissue cell, including the cell membrane and the intracellular and extracellular regions, was modelled as a spherical body. Equations for the three components in spherical coordinates were developed to calculate potassium ions flux in the presence of a stationary magnetic field. Simultaneous mathematical simulations of radial flux for potassium, calcium and chloride ions as well as membrane potential and osmotic pressure were calculated. Results obtained by computerized simulation showed that a magnetic field of 200 mT provoked some changes in cellular ionic concentration with respect to exposure time during first 30 s, which also impacted on the membrane potential and osmotic pressure values.

**K e y w o r d s:** magnetic field, ions, membrane, model, seed

### INTRODUCTION

The effects of magnetic field on post-germination processes in seeds have been studied for some time (Aladjjiyan, 2007; Flórez *et al.*, 2007; Pietruszewski *et al.*, 2007). The principal results show that some values of magnetic induction and exposure time provoke increments in germination percent, root and stem length as well as the biomass, at second week after sowing (Galland and Pazur, 2005). These effects are still waiting for clarification from the theoretical point of view because they involve numerous factors that affect germination and plant development. Modification in chlorophyll content (Taia *et al.*, 2007), peroxidase content (Atak *et al.*, 2007), increased water adsorption (Socorro and Fraga, 2007), rate growth increments at later stages of the vegetative cycle (De Souza *et al.*, 2006) and increased yield (Rochalska *et al.*, 2009) have been found experimentally. Nevertheless, exposures of different species to equal magnetic fields do not provide the same

experimental results (Pietruszewski *et al.*, 2007). Several announcements (with commercial purposes) have erroneously proposed that exposure of any biological organism to magnetic field of any strength always provides benefits to the organism (González, 2003). Although magnetic induction values below 400 mT do not provoke damage to DNA (Suzuki *et al.*, 2001), such exposure may or may not benefit living organisms: the type of magnetic field and its intensity must be taken into account. For example, stationary and variable magnetic field effects are not equal, while quantifiable values of magnetic field induction on biological tissue are relatively very low (near the nanoTesla level). On the other hand, magnetic induction values between 10 and 200 mT can interact with the flux of charged particles through the cell membrane and modify their corresponding concentrations. This in turn may affect the osmotic mechanism governing water flux (osmoregulation) (García and Arza, 2001). Increases in the cytokine and auxin synthesis have been suggested to explain lengthening of plant organs after exposure to magnetic fields (Atak *et al.*, 2003). The theory which underlies the interaction between the seed (specifically the tissues that comprise it) and a stationary magnetic field is very complex. Although several models have been proposed to explain the incidence of magnetic field on ions flux through membranes, most of these models assume a Cartesian coordinate system and perpendicularity between the magnetic field and current density (García and Arza, 2001). These assumptions limited the models capacity to simulate cellular geometry and the interactions with non-perpendicular induction lines. This paper presents a model designed to improve the simulation of cellular electric properties, including ion flux through membranes.

\*Corresponding author's e-mail: asocorro@inifat.co.cu

The seed treatment with a stationary magnetic field includes three stages. First, the seed is placed within the field such that the embryo tissue receives a magnetic flux variation during a relatively small time interval,  $\Delta t$ , ( $10^{-3}$  s approximately). In this stage, a magnetic field creates an electrical force (EF) caused by a magnetic flux variation in a time interval,  $\Delta t$ . In the second stage, the seed is held within a magnetic field during an exposure time ( $t_E$ ), ( $t_E \gg \Delta t$ ), where there is no induced electric field. In the final stage, the seed is removed from the field and is subjected once again to a magnetic flux variation, this time in an inverse direction in relation to stage I, for the same time value,  $\Delta t$ .

The spherical cell model used in this model has previously been used for the application of mathematical equations to biological phenomena in this kind of system, where the tissue is subjected to an electromagnetic field. Our model conceptualises the cell as two concentric spheres with radius  $R_1$  (from centre to inner surface) and  $R_2$  (to outside surface) (Fig. 1a). Membrane thickness is calculated as  $\delta = R_2 - R_1$ . The inner membrane is assumed to be negatively charged, and the outer surface – positively charged. The spherical coordinate system ( $r, \varphi, \theta$ ) was used, taking the centre of the cell as the coordinate system origin. The symmetry of this model allows assuming (without loss of generality) that the magnetic field is directed along the Z axis ( $\theta = 0$ ) (Fig. 1b). Vector  $B$  can be decomposed into two components  $B_r$  and  $B_\theta$  (Fig. 1c), while  $B_\varphi = 0$ .

The quantification of induced EF (stages I and III) is a non-trivial task. Nevertheless, Galland and Pazur (2005) report the presence of voltage-dependent channels through

the membranes such that EF induction could result in ionic concentration variation and perturb the electrochemistry equilibrium (in this small time interval). During stage II, the electrochemistry gradient difference drives an ionic flux and the system reaches the equilibrium again. This ionic flux is subjected to magnetic field which does not generate EF induction, but it does exert Lorentz magnetic force on charged particles in movement.

With reference to potassium, calcium and chloride ions on both sides of the membrane and under the influence of an electromagnetic field (stationary and homogeneous), the mathematical expressions for electric currents caused by the interactions are:

$$\vec{J}_K = -RT\mu_K \vec{\nabla}C_K + F\mu_K C_K \vec{E} + \mu_K \vec{J}_K \vec{B}, \quad (1)$$

$$\vec{J}_{Ca} = -RT\mu_{Ca} \vec{\nabla}C_{Ca} + 2F\mu_{Ca} C_{Ca} \vec{E} + \mu_{Ca} \vec{J}_{Ca} \vec{B}, \quad (2)$$

$$\vec{J}_{Cl} = -RT\mu_{Cl} \vec{\nabla}C_{Cl} + F\mu_{Cl} C_{Cl} \vec{E} - \mu_{Cl} \vec{J}_{Cl} \vec{B}, \quad (3)$$

where:  $J_K, J_{Ca}$  and  $J_{Cl}$  are expressed in current intensity per area unit ( $A m^2$ ),  $C_K, C_{Ca}$  and  $C_{Cl}$  are the respective concentrations with respect to the spatial coordinates ( $mol m^{-3}$ ),  $\nabla C_K, \nabla C_{Ca}$  and  $\nabla C_{Cl}$  are the respective concentration gradient vectors ( $mol m^{-4}$ ),  $\mu_K, \mu_{Ca}, \mu_{Cl}$  represent the ionic mobility for each ion ( $m^2 V^{-1} s^{-1}$ ), while  $E$  and  $B$  are electric intensity ( $m^2 V^{-1} s^{-1}$ ) and magnetic induction ( $V m^{-1}$  or Tesla), respectively.  $R$  is the gas constant ( $8.31 J mol^{-1} K^{-1}$ ) and  $T$  is the temperature.

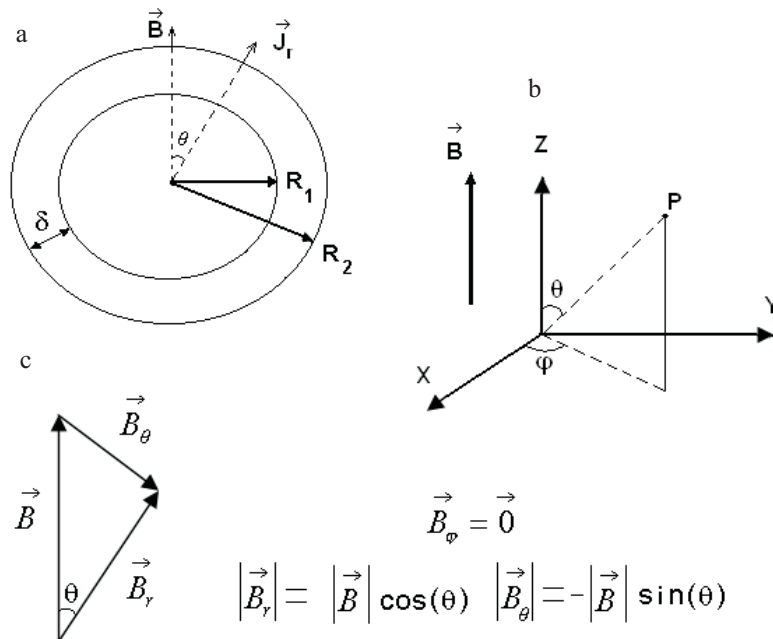


**Fig. 1.** Model scheme: a – spherical cell showing membrane thickness and vectors of radial flux and magnetic induction; b – spherical coordinates system transformation from Cartesian system, where:  $B$  is directed toward Z axis ( $\theta=0$ ); c – decomposition of  $B$  vectors for the three spherical compounds.

The first term in Eqs (1)-(3) represents a diffusion flux which depends on the concentration gradient (Glaser, 2001). The second term corresponds to the electric field action, while the third term is related to the Lorentz force. According to this formulation, the ionic flux at all angle values between  $J$  and  $B$  is considered, and not exclusively when these vectors are perpendiculars.

Electric field depends entirely on membrane potential and therefore it has only a radial component while the particles are homogeneously distributed with respect to axes  $\varphi$  and  $\theta$ . Consequently, the partial derivatives of  $C_K$ ,  $C_{Ca}$  and  $C_{Cl}$  with respect to variables  $\varphi$  and  $\theta$  are zero. After development of (1) for spherical coordinates, three equations are obtained for potassium ionic flux  $J_K$  considering the  $B$  decomposition in this kind of system (Fig. 1c):

$$J_K^{(r)} = F\mu_K C_K E^{(r)} - RT\mu_K \frac{dC_K}{dr} - \mu_K B \sin \theta J^{(\varphi)}, \quad (4)$$

$$J_K^{(\varphi)} = \mu_K B [J^{(\theta)} \cos \theta - J^{(r)} \sin \theta], \quad (5)$$

$$J_K^{(\theta)} = \mu_K B \cos \theta J^{(\varphi)}, \quad (6)$$

where:  $J_K^{(r)}$ ,  $J_K^{(\varphi)}$ , and  $J_K^{(\theta)}$  are the spherical coordinate components of  $\vec{J}_K$ . This system of equations can be solved to express each spherical component in an explicit form. For the radial axis at region  $r \approx R_1$ ,  $r \approx R_2$  (near the membrane) the result is:

$$J_K^{(r)} = J_{0K} \frac{1 + \mu^2 B^2 \cos 2\theta}{1 + \mu^2 B^2}, \quad (7)$$

where:

$$J_{0K} = - \left[ RT\mu_K \frac{dC}{dr} + F\mu_K C_K \frac{U}{\delta} \right]. \quad (8)$$

$U$  is the membrane potential and  $\delta$  the membrane thickness. Equation (7) reflects the effects of  $B$  (magnetic field induction) and  $\theta$  (angle between radial flux and  $B$ ) on the radial flux values. This expression also coincides with the specific case where the problem is subject to analysis using the Cartesian coordinates, limited to a small sector near the membrane where perpendicularity exists between  $B$  and  $J$  ( $\theta=90^\circ$ ) (García and Arza, 2001). On the other hand, Eq. (8) shows the diffusion gradient effects and electric field effects (first and second terms in Eqs (1)-(3)), where the magnetic field is absent. The ionic current,  $I$  (A) for potassium ions can be calculated by integrating the radial flux  $J$  (current density) around the entire sphere surface, using a spherical coordinate system:

$$I_K = \frac{S_K J_{0K}}{(1 + \mu^2 B^2)} \left( 1 + \frac{\mu^2 B^2}{3} \right) \quad (9)$$

where:  $S_K$  is the area occupied by potassium channels into the membrane.

Considering a small portion of membrane, the integration with respect to  $r$  from the cell interior  $C_K^{(Int)}$  ( $r = R_1$ ) toward the cell exterior  $C_K^{(Ext)}$  ( $r = R_2$ ) for each ion, Eq. (8) is converted as:

$$J_{0K} = \frac{F^2 P_K U}{RT} \frac{C_K^{(Ext)} - C_K^{(Int)} \exp\left[-\frac{FU}{RT}\right]}{\exp\left[-\frac{FU}{RT}\right] - 1}. \quad (10)$$

This expression represents the radial current density of potassium when  $B=0$ , and is known as the Nerst-Plank equation (García and Arza, 2001). For the rest of the ions (calcium and chloride) the procedure is analogous and the respective equations for ionic current are obtained:

$$I_{Ca} = \frac{S_{Ca} J_{0Ca}}{(1 + \mu^2 B^2)} \left( 1 + \frac{\mu^2 B^2}{3} \right) \quad (11)$$

$$I_{Cl} = \frac{S_{Cl} J_{0Cl}}{(1 + \mu^2 B^2)} \left( 1 + \frac{\mu^2 B^2}{3} \right) \quad (12)$$

where:

$$J_{0Ca} = \frac{2F^2 P_{Ca} U}{RT} \frac{C_{Ca}^{(Ext)} - C_{Ca}^{(Int)} \exp\left[-\frac{2FU}{RT}\right]}{\exp\left[-\frac{2FU}{RT}\right] - 1} \quad (13)$$

$$J_{0Cl} = \frac{F^2 P_{Cl} U}{RT} \frac{C_{Cl}^{(Ext)} - C_{Cl}^{(Int)} \exp\left[-\frac{FU}{RT}\right]}{\exp\left[-\frac{FU}{RT}\right] - 1} \quad (14)$$

$P_K$ ,  $P_{Ca}$  and  $P_{Cl}$  represent the membrane permeability for each of the ions. Permeability is directly proportional to ion mobility, and inversely proportional to membrane thickness (Glaser, 2001).

The seed during the latency state can be considered a living organism that neither produces nor consumes biomass. Recent papers relate the germination process to the availability of enzymes such as  $H^+$ -ATPase (Sveinsdóttir *et al.*, 2009) which increases in concentration as germination begins. During the seed latency state it is believed that there are low concentrations of ATP as well as other enzymes that promote active transport through the cell membrane. For this reason we can assume that in the seed living tissue (including the embryo) there is little or no production of ATP. This would imply the absence of active transport through the membrane (ionic pump fundamentally), which occurs with germination and cell division. Therefore, embryo cells tend to preserve their ionic concentration in specific values which

maintains the electrochemistry equilibrium between the inner and outer of the cell, and avoids ATP consumption for active transport.

The membrane potential is calculated using the Hodgkin-Katz equation, sometimes called the Goldman equation (Glaser, 2001):

$$U_{Dif} = \frac{RT}{F} \ln \left[ \frac{P_K C_K^{(Int)} + P_{Ca} C_{Ca}^{(Int)} + P_{Cl} C_{Cl}^{(Ext)}}{P_K C_K^{(Ext)} + P_{Ca} C_{Ca}^{(Ext)} + P_{Cl} C_{Cl}^{(Int)}} \right]. \quad (15)$$

This represents the electric potential difference of the membrane due to the distribution of charged particles across the membrane. Equation (15) relates the contribution of diffusible ions to the membrane potential. On the other hand, the total potential,  $U$ , must include the contribution of non-diffusible ions,  $U_{Ind}$ , which are negatively charged:

$$U = U_{Dif} + U_{Ind}. \quad (16)$$

The current density simulation (three axes in spherical coordinates) with respect to the angle between magnetic induction lines and radial flux,  $\theta$ , was done using Eqs (4), (5) and (6), for  $B=0$ , and for 100 and 200 mT. The parameters and their values used are shown in Table 1.

The radial current density was mathematically simulated for ions  $K^+$ ,  $Ca^{++}$  and  $Cl^-$  using the magnetic induction values  $B=0$  and  $B=200$  mT (Eqs (9), (11) and (12)). The ion amount (for  $K^+$ ,  $Ca^{++}$  and  $Cl^-$ ) in the cell, with respect to the exposure time,  $N(t)$ , was calculated using the ‘‘Finite Differences’’ approach to  $dN/dt$ , with a time-step of 0.1 s during 30 s. Figure 2 provides a schematic for this calculation, and Table 2 contains the parameters used in the simulation process. The relationship between  $N$  and  $t$  allowed the calculation of the respective ionic concentrations in the cell with respect to exposure time. The initial conditions and other parameters were estimated from observed data collected from other plant tissue cells.

Having obtained the ionic current values, the variation of cellular ionic concentrations during magnetic exposure can be calculated, along with the variation of membrane potential  $U$ . Data obtained for  $U$  were then used to calculate ionic flux, ionic concentration, and membrane potential as the process was continuously repeated (Fig. 2).

## RESULTS AND DISCUSSION

Figure 3 shows the current density or ionic flux in presence of a stationary magnetic field (100 and 200 mT) with respect to angle  $\theta$  in the initial instant for each spherical axis. A direct proportional relationship between magnetic field induction and total ion flux is observed. The current density components  $J_r$  and  $J_\theta$  were at their maximum values near  $\theta = \pi/2$  (maximum value for Lorentz Force), and were null at  $\theta = 0$  and  $\theta = \pi$ . For this reason other models consider only the case for  $B$  and  $J$  perpendicularly in Cartesian coordinates (García and Arza, 2001).

**Table 1.** Data used in the simulation for the three  $J_K$  components

Properties	Values
Faraday number	$0.965 \cdot 10^5 \text{ C mol}^{-1}$
Gases constant, $R$	$8.31 \text{ J mol}^{-1} \text{ K}^{-1}$
Temperature, $T$	300 K
Mobility of ion $K^+$ , $\mu_K$	$5 \text{ m}^2 \text{ V}^{-1} \text{ s}^{-1}$
Membrane potential, $U$	35.4 mV
Membrane thickness, $\delta$	1 nm
Outside concentration, $C_E$	3 mM
Inside concentration, $C_I$	1 mM
Magnetic induction, $B$	100 and 200 mT

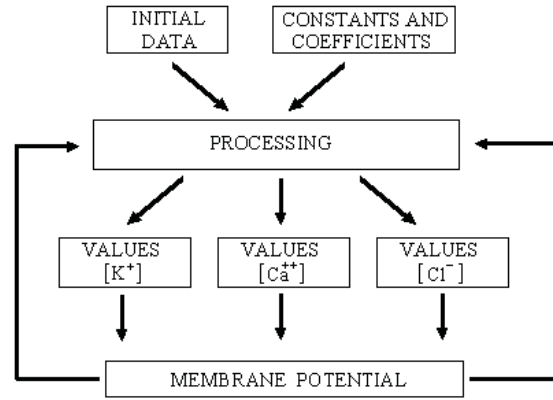


**Fig. 2.** Diagram of the recurrent calculations methodology. Initial data allow calculating radial components of  $J$  for each ion. Afterward the ionic concentration values are obtained and they impact on the membrane potential value, which in turn impacts on the processing of  $J$ .

**Table 2.** Values used for inner ionic concentration simulation and membrane potential calculation

Properties	Values
Ion mobility $Ca^{++}$ , $\mu_{Ca}$	$2.2 \text{ m}^2 \text{ V}^{-1} \text{ s}^{-1}$
Ion mobility $Cl^-$ , $\mu_{Cl}$	$1.0 \text{ m}^2 \text{ V}^{-1} \text{ s}^{-1}$
Area of channel surface, $S$	$5 \cdot 10^{-28} \text{ m}^2$
Initial cell ratio (inside), $R_1$	$4.99 \cdot 10^{-7} \text{ m}$
Initial cell ratio (outside), $R_2$	$5.00 \cdot 10^{-7} \text{ m}$
Initial conc. (inside) $K^+$ , $C_{K0}^{in}$	1.15 mM
Initial conc. (outside) $K^+$ , $C_{K0}^{Out}$	1.10 mM
Initial conc. (inside) $Ca^{++}$ , $C_{Ca0}^{in}$	1.50 mM
Initial conc. (outside) $Ca^{++}$ , $C_{Ca0}^{Out}$	1.00 mM
Initial conc. (inside) $Cl^-$ , $C_{Cl0}^{in}$	2.00 mM
Initial conc. (outside) $Cl^-$ , $C_{Cl0}^{Out}$	7.00 mM

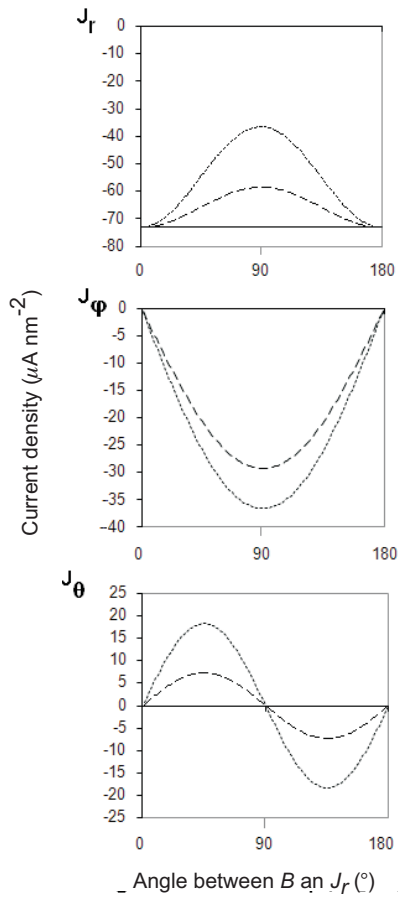


**Fig. 3.** Homogeneous and stationary magnetic field effects on current density vector  $J$  for potassium. Each graph shows the respective components at spherical coordinates. Data obtained by simulation for  $B$  values: 0 (—), 100 (---), and 200 (- - -) mT.

Nevertheless, changes in the value of  $J$  within a stationary magnetic field were found as  $\theta$  was varied from  $\theta = \pi/2$ . The biological effects of magnetic seed treatment may originate from the result of all the  $J$  values independent of  $\theta$ . The “ $r$ ” values for which the curves in Fig. 3 can be validated correspond to  $r < R_1$  or  $r > R_2$  since the movement of ions into the membrane must be approximately radial (through protein-pores). According to the Singer and Nicholson model (Lommerce *et al.*, 2004), the lipid bi-layer construction of the cell membrane hinders other transmembrane angular movement with respect to the  $\theta$  and  $\varphi$  axes.

Figure 3 shows that the orders of magnitude of the three  $J$  components for potassium ions were very similar. In this case,  $K^+$  ion mobility is higher than mobility of the other ions. On the other hand, for heavier and therefore less mobile ions, Eqs (4)-(5)-(6) confirmed a substantial decrease of ionic flux with respect to the  $\varphi$  and  $\theta$  axes, while the radial component maintains high values due to membrane electric field action. In the simulation process, the  $\varphi$  and  $\theta$  axes did not affect the intracellular concentration.

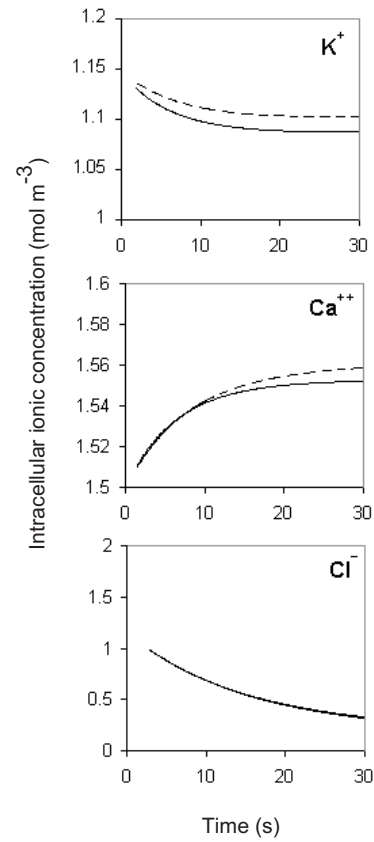


**Fig. 4.** Magnetic field effects on ionic concentration in a cell with respect to the exposure time.

Only the radial axis ionic current was considered in calculating the concentration for each of the  $K^+$ ,  $Ca^{++}$  and  $Cl^-$  ions (Fig. 4). The presence of ionic current density variation implied changes in intracellular concentration values. The dependence on exposure time ‘ $t_E$ ’ during stage II is shown for these ions. For the simulation it was assumed that the cell was not initially at the electrochemistry equilibrium state for either treatment or control. Stage I (magnetic flux variation) could vary the ionic concentration due to a speedy variation of membrane potential. At stage II, ionic concentration values varied until reaching equilibrium for both cases (stationary magnetic field for 200 mT and  $B=0$ ). Nevertheless, the values of intracellular ionic concentrations at equilibrium for magnetic exposure of  $B=200$  mT were higher than  $B=0$  between 15 and 30 s for potassium and calcium. Chloride ions did not show differences between treatment and control.

This behaviour for intracellular concentrations was accompanied by variations in membrane potential according to the Goldman Eq. (15) whose trace is shown at Fig. 5a. The simulated data show a clear difference in membrane electric potential. The  $U$  value at 30 s for  $B=200$  mT was

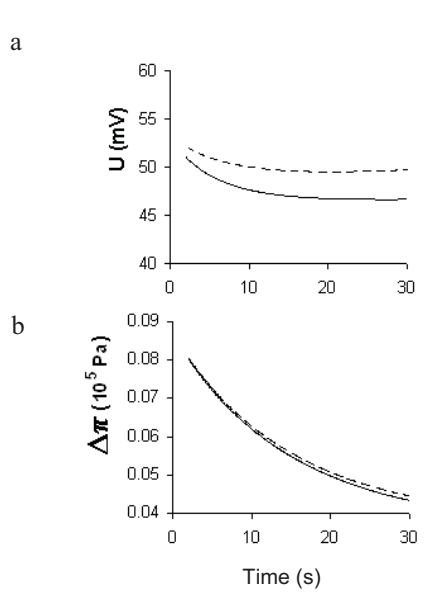


**Fig. 5.** Magnetic field effects on biophysical parameters with respect to exposure time for  $B=0$  (magnetic field absence, —) and  $B=200$  mT (magnetic field presence ---): a – membrane potential behaviour ( $U$ ), b – osmotic pressure difference ( $\Delta\pi = \pi_{inside} - \pi_{outside}$ ).

higher than  $U$  for  $B=0$ . This is related to the increase in ionic concentration which also affects the osmotic pressure difference between the cell inside and outside (Fig. 5b). The higher differences between treated and control were obtained in 10–30 s of exposure. This increase of osmotic pressure favours the water flux into the cell and could influence water absorption increases during the seed imbibition period.

The simulation model demonstrated here is capable of explaining the effects of magnetic treatment of seeds. First, intracellular ionic concentration showed variations which in turn can explain the possible change of osmotic behaviour. Second, the results can justify the effects of magnetic seed treatment through the model when the seed is placed into a hydrated medium. For this reason, chronic treatment with permanent magnets (Martinez *et al.*, 2000; 2009) has been suggested, so that the seed absorbs water while interacting with the magnetic field.

Changes in membrane permeability have been observed in *Vicia faba* using magnetic field values below 100 mT (Stange *et al.*, 2002), while other authors have explained the magnetic effects as due to variations of the induced ionic current across the cellular membrane, which results in variations in the osmotic pressure (García *et al.*, 2001). These results could be relevant to explain physiological changes found in post-germination parameters for soybean and some other crops (Atak *et al.*, 2003; Parsi, 2007). The results of this simulation showed that  $Ca^{++}$  concentration was affected by the magnetic treatment at 200 mT during the first seconds of magnetic field interaction. This is important since calcium ions are related to enzymes which participate in several metabolic reactions during the germination process.

The calculation of ionic diffusion through the membrane was based on principles from the Goldman-Hodgkin-Katz (GHK) theory which assumes (among other things) that the electric field into the channel is constant with respect to the geometry and spatial coordinates used. This in turn permits the assumption that the interaction between ions and electrically charged biological molecules (polar amino-acid) is negligible. Experimentation has demonstrated that the GHK theory is not completely correct and additional models are needed to explain charged particle flux through biological membranes. Nevertheless, these results are useful to the extent that variation of membrane potential due to a magnetic field is much lower than the initial  $U$  value of the cell.

The intent of this study was not to quantitatively evaluate the bioelectromagnetic mechanisms that affect concentration values in stages I and III. Rather, it assumes that physiological effects are caused by the modifications occurring at stage II, when biophysical parameters vary with respect to exposure time in the presence of magnetic field. When the magnetic field is removed at stage III an electric field is induced, although its intensity is not equal to that of the electric field at stage I. This could be caused by differences in ionic conductance in each direction, due to imperfections in the channel morphology and the heterogeneity of the amino-acid polarity in those pores. Another difficulty in simulating stages I and III is the opposite nature of the magnetic field in each of the two semi-spheres. For this reason we assumed a non-homogeneous distribution of channels around the cell surface.

The simulation results showed that during interactions between the cell sphere and the magnetic field, ionic concentration variations with respect to the exposure time are different when magnetic field is removed. In all cases the simulated data curves showed magnetic field effects on calculated variables, with substantial variations during the first 30 s of exposure. Experimental results have demonstrated stimulant effects on seed through magnetic seed treatment. For example, Dziwulska-Hunek *et al.* (2009) obtained an increase in amaranth seed germination with a magnetic field of  $B = 30$  mT during 30 s. Although this data simulation was carried out for 30 s, it is plausible that this exposure was sufficient to provoke an osmotic change which would stimulate metabolic activity. Furthermore, this suggests the need for experimental research concerning magnetic effects on post-germination physiological parameters, using relatively small exposure time values, which are very practical for treatment of large amounts of seeds.

The proposed model begins with Eqs (1)–(3) where temperature has a notable effect on the ionic current density. For this reason temperature should influence the model results in the same way that temperature has influenced the magnetic effects on seed in experimental results obtained (Dziwulska-Hunek *et al.*, 2009). Other considerations regarding temperature as well as other theoretical aspects should be considered for improving the ability to simulate magnetic effects on seed.

## CONCLUSIONS

1. The proposed spherical model allows the explanation of the magnetic fields effects on ion currents for all the values of angle between flux density and magnetic induction lines ( $\theta$ ). The values of flux density are maximum at  $\theta = 90^\circ$  which corresponds to the specific case considered by previous one-dimensional models.

2. The ion flux simulation showed increments of intracellular ion concentrations for potassium and calcium while for chloride this behaviour was not observed.

3. The simulation showed electric susceptibility of the cell membrane to magnetic fields.

4. The variation of cell osmotic pressure, obtained by simulation during the first 30 s of exposure time, could explain the effects on water absorption at seeds treated with magnetic field.

## REFERENCES

- Aladjajjiyan A., 2007.** The use of physical methods for plant growing stimulation in Bulgaria. *J. Central Eur. Agric.*, 8(3), 369-380.
- Atak C., Celik O., Olgun A., Alikamanoglu S., and Rzakoulieva A., 2007.** Effect of magnetic field on peroxidase activities of soybean tissue culture. *Biotechnol. Biotechnol. EQ*, 21, 166-171.
- Atak C., Emiroglu O., Alikamanoglu S., and Rzakoulieva A., 2003.** Stimulation of regeneration by magnetic field in soybean (*Glycine max* Merrill) tissue cultures. *J. Cell Molecular Biol.*, 2, 113-119.
- De Souza A., García D., Sueiro L., Gilart F., Porrás E., and Licea L., 2006.** Pre-sowing magnetic treatments of tomato seeds increase the growth and yield of plants. *Bioelectromagnetics*, 27, 247-257.
- Dziwulska-Hunek A., Kornarzyński K., Matwijczuk A., Pietruszewski S., and Szot B., 2009.** Effect of laser and variable magnetic field simulation on amaranth seeds germination. *Int. Agrophysics*, 23, 229-235.
- Galland P. and Pazur A., 2005.** Magnetoreception in plants. *J. Plant Res.*, 118, 371-389.
- García F. and Arza L., 2001.** Influence of a stationary magnetic field on water relations in lettuce seeds. Part I: Theoretical considerations. *Bioelectromagnetics*, 22, 589-595.
- García F., Arza L., and Almanza I., 2001.** Influence of a stationary magnetic field on water relations in lettuce seeds. II: Experimental results. *Bioelectromagnetics*, 22, 596-602.
- Glaser R., 2001.** *Biophysics*. Springer Press, Heidelberg, Germany.
- González A., 2003.** Magnetism and pseudoscience in medicine (in Spanish). *Cuban J. Physics*, 20(1), 59-64.
- Flórez M., Carbonell M.V., and Martínez E., 2007.** Exposure of maize seeds to stationary magnetic fields: Effects on germination and early growth. *Environ. Exp. Botany*, 59(1), 68-75.
- Lommerse P.H.M., Spaink H.P., and Schmidt T., 2004.** *In vivo* plasma membrane organization: results of biophysical approaches. *Biochimica Biophysica Acta*, 1664, 119-131.
- Martínez E., Carbonell M.V., Flórez M., Amaya J.M., and Maqueda R., 2009.** Germination of tomato seeds (*Lycopersicon esculentum* L.) under magnetic field. *Int. Agrophysics*, 23, 44-50.
- Parsi N., 2007.** Electromagnetic effects on soybeans. MSc. Thesis, Faculty of the Graduate School, University of Missouri, Columbia, MO, USA.
- Pietruszewski S., Muszynski S., and Dziwulska A., 2007.** Electromagnetic fields and electromagnetic radiation as non-invasive external stimulant for seeds (selected methods and responses). *Int. Agrophysics*, 21, 95-100.
- Rochalska M., Grabowska K., and Ziarnik A., 2009.** Impact of low frequency magnetic fields on yield and quality of sugar beet. *Int. Agrophysics*, 23, 163-174.
- Socorro A. and Fraga N., 2007.** Seed's magnetic treatment effects on viability and longevity (in Spanish). *Tecnología Química*, 24, 86-92.
- Stange B.C., Rowland R.E., Rapley B.I., and Podd J.V., 2002.** ELF magnetic field increase aminoacid uptake into *Vicia faba* L. roots and alter ion movement across the plasma membrane. *Bioelectromagnetics*, 33, 347-354.
- Suzuki Y., Ikehata M., Nakamura K., Nishioka M., Asanuma K., Koana T., and Shimizu H., 2001.** Induction of micronuclei in mice exposed to static magnetic fields. *Mutagenesis*, 16(6), 499-501.
- Sveinsdóttir H., Yan F., Zhu Y., Peiter-Volk T., and Schubert S., 2009.** Seed ageing-induced inhibition of germination and post-germination root growth is related to lower activity of plasma membrane H<sup>+</sup>-ATPase in maize roots. *J. Plant Physiology*, 166(2), 128-135.
- Taia W.K., Al-Zahrani H.S., and Kotbi A.M., 2007.** The effect of static magnetic field forces on water content and photosynthetic pigments in sweet basil *Ocimum basilicum* L. (*Lamiaceae*). *Saudi J. Biol. Sci.*, 14(1), 103-107.